J|A|C|S ARTICLES

Published on Web 06/22/2010

A Proton-Shuttle Reaction Mechanism for Histone Deacetylase 8 and the Catalytic Role of Metal Ions

Ruibo Wu,[†,‡] Shenglong Wang,[†] Nengjie Zhou,[†] Zexing Cao,[‡] and Yingkai Zhang*[,†]

Department of Chemistry, New York University, New York, New York 10003, and Department of Chemistry and State Key Laboratory of Physical Chemistry of Solid Surfaces, College of Chemistry and Chemical Engineering, Xiamen University, Xiamen 361005, China

Received May 8, 2010; E-mail: yingkai.zhang@nyu.edu

Abstract: Zinc-dependent histone deacetylase 8 (HDAC8) catalyzes the removal of acetyl moieties from histone tails, and is critically involved in regulating chromatin structure and gene expression. The detailed knowledge of its catalytic process is of high importance since it has been established as a most promising target for the development of new antitumor drugs. By employing Born−Oppenheimer ab initio QM/MM molecular dynamics simulations and umbrella sampling, a state-of-the-art approach to simulate enzyme reactions, we have provided further evidence against the originally proposed general acid−base catalytic pair mechanism for Zinc-dependent histone deacetylases. Instead, our results indicated that HDAC8 employs a proton-shuttle catalytic mechanism, in which a neutral His143 first serves as the general base to accept a proton from the zinc-bound water molecule in the initial rate-determining nucleophilic attack step, and then shuttles it to the amide nitrogen atom to facilitate the cleavage of the amide bond. During the deacetylation process, the Zn^{2+} ion changes its coordination mode and plays multiple catalytic roles. For the K^+ ion, which is located about 7 Å from the catalytic Zn^{2+} ion and conserved in class I and II HDACs, our simulations indicated that its removal would lead to the different transition state structure and a higher free energy reaction barrier for the rate-determining step. It is found that the existence of this conserved K^+ ion would enhance the substrate binding, increase the basicity of His143, strengthen the catalytic role of zinc ion, and improve the transition state stabilization by the enzyme environment.

1. Introduction

The acetylation state of lysine residues in proteins has emerged as a vital regulator in complex cellular processes.[1−3] The removal of acetyl groups from acetyl-lysine residues of histone tails often leads to a closed chromatin structure and is generally associated with transcriptional repression and gene silencing.[4] Enzymes responsible for catalyzing this pivotal deacetylation process are histone deacetylases (HDACs),[5−9] which have been divided into four classes based on phylogenetic analyses.[10] Among them, Class I, II and IV HDACs are zinc dependent hydrolases, while the third class of deacetylases are NAD^+ dependent sirtuins and do not contain a catalytic zinc site. The aberrant overexpression of zinc-dependent HDACs has been mechanistically linked to a variety of diseases, and their inhibitors have emerged as a novel promising class of anticancer agents.[6,11−15] In 2006, an HDAC inhibitor SAHA which is directly coordinated to the catalytic zinc ion has been approved as an anticancer drug by FDA.[11,14] Thus, the detailed knowledge of catalytic mechanism of zinc-dependent HDACs is not only of great fundamental interest, but also of high medical importance since it would facilitate the development of new mechanism-based and subtype specific HDAC inhibitors.[15−20]

[†] New York University.
[‡] Xiamen University.

(1) Kouzarides, T. *Cell* **2007**, *128*, 693–705.
(2) Wang, Z. B.; Zang, C. Z.; Rosenfeld, J. A.; Schones, D. E.; Barski, A.; Cuddapah, S.; Cui, K. R.; Roh, T. Y.; Peng, W. Q.; Zhang, M. Q.; Zhao, K. *J. Nat. Genet.* **2008**, *40*, 897–903.
(3) Yang, X. J.; Seto, E. *Oncogene* **2007**, *26*, 5310–5318.
(4) Gallinari, P.; Di Marco, S.; Jones, P.; Pallaoro, M.; Steinkuhler, C. *Cell Res.* **2007**, *17*, 195–211.
(5) Finnin, M. S.; Donigian, J. R.; Cohen, A.; Richon, V. M.; Rifkind, R. A.; Marks, P. A.; Breslow, R.; Pavletich, N. P. *Nature* **1999**, *401*, 188–193.
(6) Haberland, M.; Montgomery, R. L.; Olson, E. N. *Nat. Rev. Genet.* **2009**, *10*, 32–42.
(7) Hodawadekar, S. C.; Marmorstein, R. *Oncogene* **2007**, *26*, 5528–5540.
(8) Yang, X. J.; Seto, E. *Nat. Rev. Mol. Cell Biol.* **2008**, *9*, 206–218.
(9) Smith, B. C.; Denu, J. M. *Biochim. Biophys. Acta, Gene Regul. Mech.* **2009**, *1789*, 45–57.
(10) Gregoretti, I. V.; Lee, Y. M.; Goodson, H. V. *J. Mol. Biol.* **2004**, *338*, 17–31.
(11) Bolden, J. E.; Peart, M. J.; Johnstone, R. W. *Nat. Rev. Drug Discovery* **2006**, *5*, 769–784.
(12) Kazantsev, A. G.; Thompson, L. M. *Nat. Rev. Drug Discovery* **2008**, *7*, 854–868.
(13) Paris, M.; Porcelloni, M.; Binaschi, M.; Fattori, D. *J. Med. Chem.* **2008**, *51*, 1505–1529.
(14) Marks, P. A.; Breslow, R. *Nat. Biotechnol.* **2007**, *25*, 84–90.
(15) Bradner, J. E.; West, N.; Grachan, M. L.; Greenberg, E. F.; Haggarty, S. J.; Warnow, T.; Mazitschek, R. *Nat. Chem. Biol.* **2010**, *6*, 238–243.
(16) Estiu, G.; Greenberg, E.; Harrison, C. B.; Kwiatkowski, N. P.; Mazitschek, R.; Bradner, J. E.; Wiest, O. *J. Med. Chem.* **2008**, *51*, 2898–2906.
(17) Suzuki, N.; Suzuki, T.; Ota, Y.; Nakano, T.; Kurihara, M.; Okuda, H.; Yamori, T.; Tsumoto, H.; Nakagawa, H.; Miyata, N. *J. Med. Chem.* **2009**, *52*, 2909–2922.
(18) Liu, T.; Kapustin, G.; Etzkorn, F. A. *J. Med. Chem.* **2007**, *50*, 2003–2006.
(19) Balasubramanian, S.; Verner, E.; Buggy, J. *J. Cancer Lett.* **2009**, *280*, 211–221.
(20) Olsen, C. A.; Ghadiri, M. R. *J. Med. Chem.* **2009**, *52*, 7836–46.

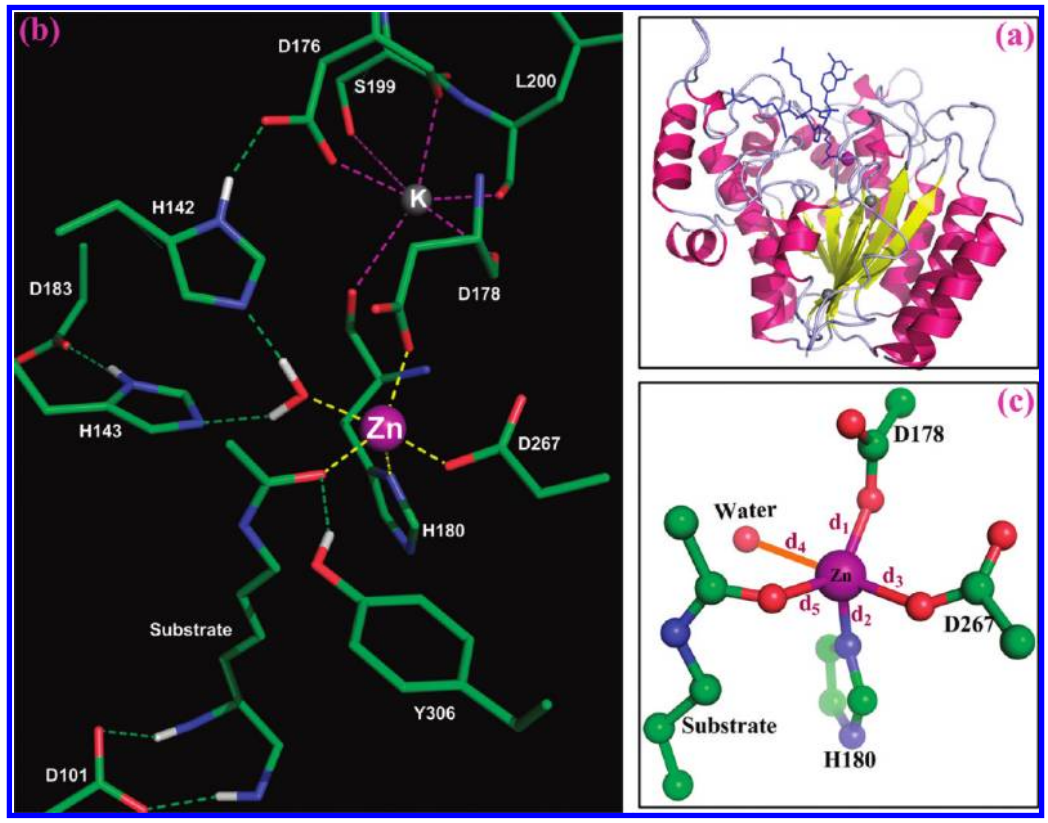

Figure 1. (a) Illustration of the HDAC8 enzyme−substrate complex structure. Zn^{2+} ion is colored in purple, K^+ ion in gray, and substrate in blue. (b) Illustration of the active site structure of HDAC8 ES complex. The K^+ coordination shell is indicated by dash lines in purple, and the important hydrogen bonds are shown by dash lines in green. (c) The zinc coordination shell in the active site. The Zn−water coordination distance (d_4) is shown in orange.

Among zinc-dependent HDACs, human zinc-dependent histone deacetylase 8 (HDAC8) lies on the evolutionary boundary between class I and class II HDACs,[10] and has become the best characterized experimentally.[21−27] Recently, structures of several HDAC8 enzyme−inhibitor and mutant−substrate complexes have been determined,[22−25] which have a similar catalytic core structure and active site as a histone deacetylase like protein (HDLP),[5,22] an archaeal homologue of eukaryotic deacetylases. The catalytic zinc ion in the active site of HDAC8−substrate complex[24] is fivefold coordinated to one His, two Asp residues, one water molecule, and the carbonyl-oxygen atom of the acetyllysine, as shown in Figure 1. The residues in its second coordination sphere include Tyr306, Asp101, His142−Asp176, and His143−Asp183 dyads, which are conserved among class-I HDACs and HDLP.[5,28] In spite of their highly conserved catalytic domain, one key structural difference between HDAC8 and HDLP is that the former has two K^+ ion binding sites[22−25] while the latter lacks these.[5] One K^+ ion is located at site 1 which is ~7 Å away from the zinc ion in HDAC8, while the other site 2 is positioned much toward the periphery. The K^+ ion of site 1, as shown in Figure 1, interacts closely with the zinc catalytic site. Intriguingly, this potassium binding site is conserved across all zinc-dependent HDACs,[23] and has been hypothesized to influence the deacetylation reaction in various ways.[22,23,27]

For the deacetylation process catalyzed by HDAC8, several different catalytic mechanisms have been proposed in the literature.[9,29] The original one is a general acid−base catalytic pair mechanism, which was first hypothesized based on structural studies of HDLP.[5] As shown in Scheme 1 of Figure 2, a singly protonated His142 serves as a general base to abstract a proton from the zinc-bound water ligand to facilitate the first nucleophilic attack reaction step, and a doubly protonated His143 is a general acid to protonate the leaving group in the second amide bond cleavage step.[5,7] However, our previous DFT QM/MM studies on HDLP did not support this originally proposed mechanism, and suggested a lower protonation state for the active site and an unconventional proton-shuttle catalytic mechanism,[30] shown as Scheme 2 in Figure 2. In this proton-shuttle mechanism[30] which has subsequently guided the design and development of a novel class of HDAC inhibitors,[17] both His142 and His143 are singly protonated in the enzyme−substrate reactant complex, and His143 serves as the general base and general acid to shuttle the proton to the leaving group.[30] It should

(21) De Ruijter, A. J. M.; Van Gennip, A. H.; Caron, H. N.; Kemp, S.; Van Kuilenburg, A. B. P. *Biochem. J.* **2003**, *370*, 737–749.
(22) Somoza, J. R.; et al. *Structure* **2004**, *12*, 1325–1334.
(23) Vannini, A.; Volpari, C.; Filocamo, G.; Casavola, E. C.; Brunetti, M.; Renzoni, D.; Chakravarty, P.; Paolini, C.; De Francesco, R.; Gallinari, P.; Steinkuhler, C.; Di Marco, S. *Proc. Natl. Acad. Sci. U.S.A.* **2004**, *101*, 15064–15069.
(24) Vannini, A.; Volpari, C.; Gallinari, P.; Jones, P.; Mattu, M.; Carfi, A.; De Francesco, R.; Steinkuhler, C.; Di Marco, S. *EMBO Rep.* **2007**, *8*, 879–884.
(25) Dowling, D. P.; Gantt, S. L.; Gattis, S. G.; Fierke, C. A.; Christianson, D. W. *Biochemistry* **2008**, *47*, 13554–13563.
(26) Gantt, S. L.; Gattis, S. G.; Fierke, C. A. *Biochemistry* **2006**, *45*, 6170–6178.
(27) Gantt, S. L.; Joseph, C. G.; Fierke, C. A. *J. Biol. Chem.* **2010**, *285*, 6036–6043.
(28) Nielsen, T. K.; Hildmann, C.; Dickmanns, A.; Schwienhorst, A.; Ficner, R. *J. Mol. Biol.* **2005**, *354*, 107–120.
(29) Anzellotti, A. I.; Farrell, N. P. *Chem. Soc. Rev.* **2008**, *37*, 1629–1651.
(30) Corminboeuf, C.; Hu, P.; Tuckerman, M. E.; Zhang, Y. K. *J. Am. Chem. Soc.* **2006**, *128*, 4530–4531.

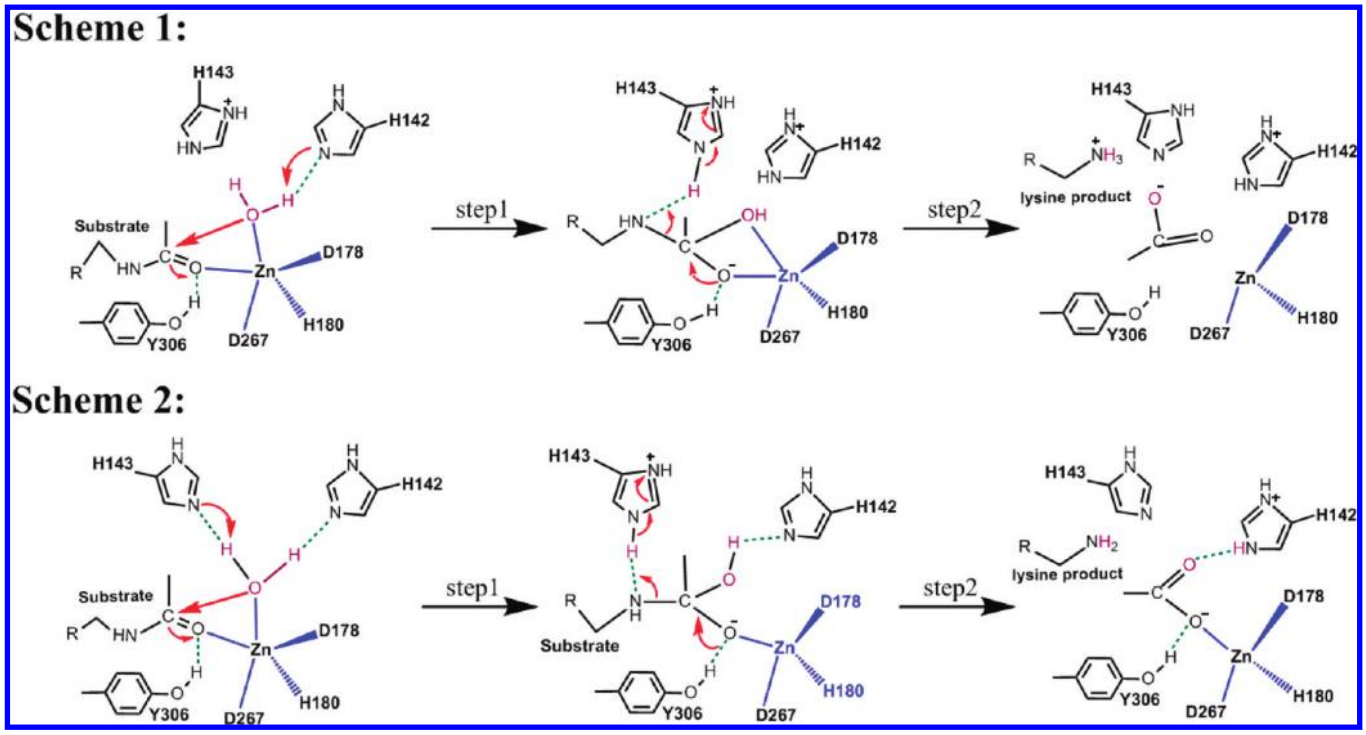

Figure 2. Two previously suggested deacetylation reaction mechanisms for class I/II/IV HDACs and HDLP (residue ID is base on the HDAC8). Scheme 1: a general acid-base catalytic pair mechanism, which was first hypothesized based on structural studies of HDLP.[5] Scheme 2: a proton-shuttle catalytic mechanism which was suggested based on the previous DFT QM/MM studies of HDLP.[30]

be noted that this previous DFT QM/MM study[30] was based on the crystal structure of an HDLP−SAHA complex (PDB ID: 1C3S[5]), in which the sole metal ion is the catalytic Zinc ion. In other QM studies[31−34] of active site models of Zinc-dependent HDACs, the K^+ ion near the active site of HDAC8 had not been taken into account either. Thus, in light of the new structural features and medical significance of HDAC8[21−27] as well as new methodology advances in simulating enzyme reactions,[35−43] a detailed theoretical characterization of HDAC8 catalytic mechanism and the functional role of the K^+ ion in site 1 is much needed.

Here, our computational studies are based on a recently determined crystal structure of the Y306F HDAC8 mutant−substrate complex.[24] The employed theoretical approaches center on Born−Oppenheimer ab initio QM/MM molecular dynamics simulations with umbrella sampling, a state-of-the-art approach to simulate enzyme reactions. It allows for a first-principle description of chemical bond formation/breaking and dynamics of the metal active site, while properly including effects of the heterogeneous and fluctuating protein environment. Our simulations have characterized the deacylation reaction mechanism of HDAC8, determined its complete free energy reaction profile, and elucidated functional roles of Zn^{2+} and K^+ ions.

2. Computational Methods

2.1. Preparation of the Simulation System. The initial structure of the enzyme−substrate complex was prepared on the basis of a recently determined crystal structure of the Y306F HDAC8 mutant−substrate complex (pdb code: 2V5W[24]). First, the mutated residue was changed back into the wild-type one with the Swiss-PdbViewer.[44] The protonation states of charged residues were determined via H++ program[45] and by carefully examining their individual local hydrogen bond networks. As Figure 1 shows, His180 was determined as singly protonated on δ site, while His143 and His142 were determined as singly protonated on ε site. To more carefully examine the protonation states of His142 and His143, we have also prepared two other structures with either His142 or His143 doubly protonated. Each prepared system was neutralized by adding Na^+ ion at the protein surface with the Amber tool, and was solvated into a rectangular box with a 10 Å buffer distance between the solvent box wall and the nearest solute atoms. Each resulting system consists of ~46 000 atoms. By employing AMBER10 molecular dynamics package,[46] it was first minimized

(31) Vanommeslaeghe, K.; Van Alsenoy, C.; De Proft, F.; Martins, J. C.; Tourwe, D.; Geerlings, P. *Org. Biomol. Chem.* **2003**, *1*, 2951–2957.
(32) Vanommeslaeghe, K.; De Proft, F.; Loverix, S.; Tourwe, D.; Geerlings, P. *Bioorg. Med. Chem.* **2005**, *13*, 3987–3992.
(33) Vanommeslaeghe, K.; Loverix, S.; Geerlings, P.; Tourwe, D. *Bioorg. Med. Chem.* **2005**, *13*, 6070–6082.
(34) Wang, D. F.; Helquist, P.; Wiest, O. *J. Org. Chem.* **2007**, *72*, 5446–5449.
(35) Wang, S. L.; Hu, P.; Zhang, Y. K. *J. Phys. Chem. B* **2007**, *111*, 3758–3764.
(36) Hu, P.; Wang, S.; Zhang, Y. *J. Am. Chem. Soc.* **2008**, *130*, 3806–3813.
(37) Hu, P.; Wang, S. L.; Zhang, Y. K. *J. Am. Chem. Soc.* **2008**, *130* (49), 16721–16728.
(38) Lu, Z. Y.; Zhang, Y. K. *J. Chem. Theory Comput.* **2008**, *4*, 1237–1248.
(39) Ke, Z. H.; Wang, S. L.; Xie, D. Q.; Zhang, Y. K. *J. Phys. Chem. B* **2009**, *113*, 16705–16710.
(40) Ke, Z. H.; Zhou, Y. Z.; Hu, P.; Wang, S. L.; Xie, D. Q.; Zhang, Y. K. *J. Phys. Chem. B* **2009**, *113*, 12750–12758.
(41) Zheng, H.; Wang, S. L.; Zhang, Y. K. *J. Comput. Chem.* **2009**, *30*, 2706–2711.
(42) Fahie, K.; Hu, P.; Swatkoski, S.; Cotter, R. J.; Zhang, Y. K.; Wolberger, C. *FEBS J.* **2009**, *276*, 7159–7176.
(43) Wu, R. B.; Hu, P.; Wang, S. L.; Cao, Z. X.; Zhang, Y. K. *J. Chem. Theory Comput.* **2010**, *6*, 337–343.
(44) Guex, N.; Peitsch, M. C. *Electrophoresis* **1997**, *18*, 2714–2723.
(45) Gordon, J. C.; Myers, J. B.; Folta, T.; Shoja, V.; Heath, L. S.; Onufriev, A. *Nucleic Acids Res.* **2005**, *33*, W368–W371.
(46) Case, D. A.; et al. *AMBER 10*, University of California: San Francisco, CA., 2008.

and equilibrated, and then simulated for 3 ns with periodic boundary condition, temperature at 300 K, and pressure at 1 atm. The trajectory was stable, and the resulted snapshot was employed for preparing subsequent QM/MM studies. The Amber99SB[47−49] force field for the protein and TIP3P model[50] for water molecules were employed, and the force field parameters for acetyl-lysine was generated from AMBER GAFF force field[51] via AMBER tools. The Zn^{2+} ion was modeled with the Stote's scheme,[52] and 1500 kcal/(mol/Å) harmonic restraint was placed on ∼15 atoms in the zinc bind site to retain the zinc coordination structure during the MM minimizations and dynamics simulations since zinc coordination shell is very difficult to be properly described by a molecular mechanical force field.[53−56]

2.2. Born−Oppenheimer Ab Initio QM/MM MD Simulations. With the snapshot taken from the classical MD trajectory, the QM/MM model was prepared by deleting solvent molecules beyond 30 Å of the zinc atom. The resulting system had ∼13 000 atoms in total, and it was partitioned into QM and MM subsystems, as illustrated in Figure S1. The QM subsystem, including the side chains of His142, His143, Asp178, His180, Asp267, substrate, water, and zinc ion, was treated by the B3LYP functional with Stuttgart ECP/basis set[57] (SDD) for the zinc atom and 6-31G* basis set for all other QM atoms. This B3LYP(SDD,6-31G*) level of QM treatment has been previously tested and employed successfully to describe zinc coordination shell,[30,43,58−61] and it is similar to that used in other contemporary ab initio QM/MM studies of Zinc enzymes.[62,63] The QM/MM boundaries were described by the pseudobond approach[64−67] with the improved parameters. All other atoms were described by the same molecular mechanical force field used in previous classical MD simulations. The prepared QM/MM system was first minimized, and then employed to map out a minimum energy path with the reaction coordinate driving method[66] and B3LYP(SDD,6-31G*) QM/MM calculations. For each determined structure along the reaction path, the MM subsystem was further equilibrated with 500 ps molecular mechanical MD simulations with the QM subsystem fixed. Then, the resulting snapshots were used as starting structures for ab initio QM/MM MD simulations with umbrella sampling. Each window was simulated for 25 ps, and in total, about 1.5 ns ab initio QM/MM MD simulations have been carried out to characterize the overall deacetylation reaction catalyzed by HDAC. The configurations after 5 ps for each window were collected for data analysis. The probability distributions along the reaction coordinate were determined for each window and pieced together with the WHAM[68,69] to calculate the free energy profile. This computational protocol has successfully been applied to study several enzymes as well as chemical reactions in aqueous solution.[35−41,43]

All our ab initio QM/MM calculations were performed with modified Q-Chem[70] and Tinker[71] programs. For all QM/MM calculations, the spherical boundary condition was applied and the atoms more than 22 Å away from the zinc atom were fixed. The 18 and 12 Å cutoffs were employed for electrostatic and van der Waals interactions, respectively. There was no cutoff for electrostatic interactions between QM and MM regions. The Beeman algorithm[72] was used to integrate the Newton equations of motion with the time step of 1 fs, and the Berendsen thermostat method[73] was employed to control the system temperature at 300 K.

3. Results and Discussion

3.1. Michaelis Reactant Complex. One key difference among previously suggested mechanisms for HDACs is the protonation state of histidine residues in two His−Asp dyads at the Michaelis reactant complex. In the case of HDAC8, three probable reactant states can be suggested. The first is the HID142/HID143 state in which both histidine residues are singly protonated, as shown in Scheme 2 of Figure 2. The second is the HIP142/HID143 state in which His142 is doubly protonated and His143 is singly protonated. The third is the HID142/HIP143 state in which His142 is singly protonated and His143 is doubly protonated, as shown in Scheme 1 of Figure 2. Here, in order to examine all these three possible states on an equal footing, we have prepared three corresponding models based on the same structure and investigated them with the same computational simulation protocol.

As shown in Figure 3, for both HIP142/HID143 and HID142/HIP143 models, the water molecule moves away from Zinc during the B3LYP(SDD,6-31G*) QM/MM MD simulations, which leads to the fourfold Zn coordinated structure. The distances between the zinc ion and the water oxygen are 3.81 ± 0.94 and 3.24 ± 0.88 Å, respectively, which is more than 1 Å longer than the corresponding distance of 2.238 Å in the crystal structure of Y306F−HDAC8−substrate complex.

Only for the HID142/HID143 model, its fivefold Zn coordinated shell is stable during simulations, and its active site structure is stable and very similar to the one in the crystal structure, as shown in Figure 3. The water molecule is coordinated to Zinc with an average distance of 2.24 ± 0.19 Å, and forms two hydrogen bonds with both His142 and His143. To provide quantitative insights into the water coordination to Zinc in the HID142/HID143 model, we have also carried out ab initio QM/MM MD simulations and umbrella sampling along

(47) Cornell, W. D.; Cieplak, P.; Bayly, C. I.; Gould, I. R.; Merz, K. M.; Ferguson, D. M.; Spellmeyer, D. C.; Fox, T.; Caldwell, J. W.; Kollman, P. A. *J. Am. Chem. Soc.* **1995**, *117*, 5179–5197.
(48) Wang, J. M.; Cieplak, P.; Kollman, P. A. *J. Comput. Chem.* **2000**, *21*, 1049–1074.
(49) Hornak, V.; Abel, R.; Okur, A.; Strockbine, B.; Roitberg, A.; Simmerling, C. *Proteins: Struct., Funct., Bioinf.* **2006**, *65*, 712–725.
(50) Jorgensen, W. L.; Chandrasekhar, J.; Madura, J. D.; Impey, R. W.; Klein, M. L. *J. Chem. Phys.* **1983**, *79*, 926–935.
(51) Wang, J. M.; Wolf, R. M.; Caldwell, J. W.; Kollman, P. A.; Case, D. A. *J. Comput. Chem.* **2004**, *25*, 1157–1174.
(52) Stote, R. H.; Karplus, M. *Proteins: Struct., Funct., Genet.* **1995**, *23*, 12–31.
(53) Liang, J. Y.; Lipscomb, W. N. *Proc. Natl. Acad. Sci. U.S.A.* **1990**, *87*, 3675–3679.
(54) Pang, Y. P. *Proteins* **2001**, *45*, 183–189.
(55) Karjiban, R. A.; Rahman, M. B. A.; Basri, M.; Salleh, A. B.; Jacobs, D.; Wahab, H. A. *Protein J.* **2009**, *28*, 14–23.
(56) Yan, C. L.; Xiu, Z. L.; Li, X. H.; Li, S. M.; Hao, C.; Teng, H. *Proteins: Struct., Funct., Bioinf.* **2008**, *73*, 134–149.
(57) Dolg, M.; Wedig, U.; Stoll, H.; Preuss, H. *J. Chem. Phys.* **1987**, *86*, 866–872.
(58) Sousa, S. F.; Fernandes, P. A.; Ramos, M. J. *J. Am. Chem. Soc.* **2007**, *129*, 1378–1385.
(59) Sousa, S. F.; Fernandes, P. A.; Ramos, M. J. *Biophys. J.* **2005**, *88*, 483–494.
(60) Xiao, C. Y.; Zhang, Y. K. *J. Phys. Chem. B* **2007**, *111*, 6229–6235.
(61) Sousa, S. F.; Fernandes, P. A.; Ramos, M. J. *Proteins: Struct., Funct., Bioinf.* **2007**, *66*, 205–218.
(62) Xu, D. G.; Guo, H. *J. Am. Chem. Soc.* **2009**, *131*, 9780–9788.
(63) Blumberger, J.; Lamoureux, G.; Klein, M. L. *J. Chem. Theory Comput.* **2007**, *3*, 1837–1850.
(64) Zhang, Y. K. *Theor. Chem. Acc.* **2006**, *116*, 43–50.
(65) Zhang, Y. K.; Lee, T. S.; Yang, W. T. *J. Chem. Phys.* **1999**, *110*, 46–54.
(66) Zhang, Y. K.; Liu, H. Y.; Yang, W. T. *J. Chem. Phys.* **2000**, *112*, 3483–3492.
(67) Zhang, Y. K. *J. Chem. Phys.* **2005**, *122*, 024114.
(68) Souaille, M.; Roux, B. *Comput. Phys. Commun.* **2001**, *135*, 40–57.
(69) Kumar, S.; Bouzida, D.; Swendsen, R. H.; Kollman, P. A.; Rosenberg, J. M. *J. Comput. Chem.* **1992**, *13*, 1011–1021.
(70) Shao, Y.; et al., *Q-Chem, version 3.0*; Q-chem, Inc.: Pittsburgh, PA, 2006.
(71) Ponder, J. W. *TINKER, Software Tools for Molecular Design*, Version 4.2; 2004.
(72) Beeman, D. *J. Comput. Phys.* **1976**, *20*, 130–139.
(73) Berendsen, H. J. C.; Postma, J. P. M.; Vangunsteren, W. F.; Dinola, A.; Haak, J. R. *J. Chem. Phys.* **1984**, *81* (8), 3684–3690.

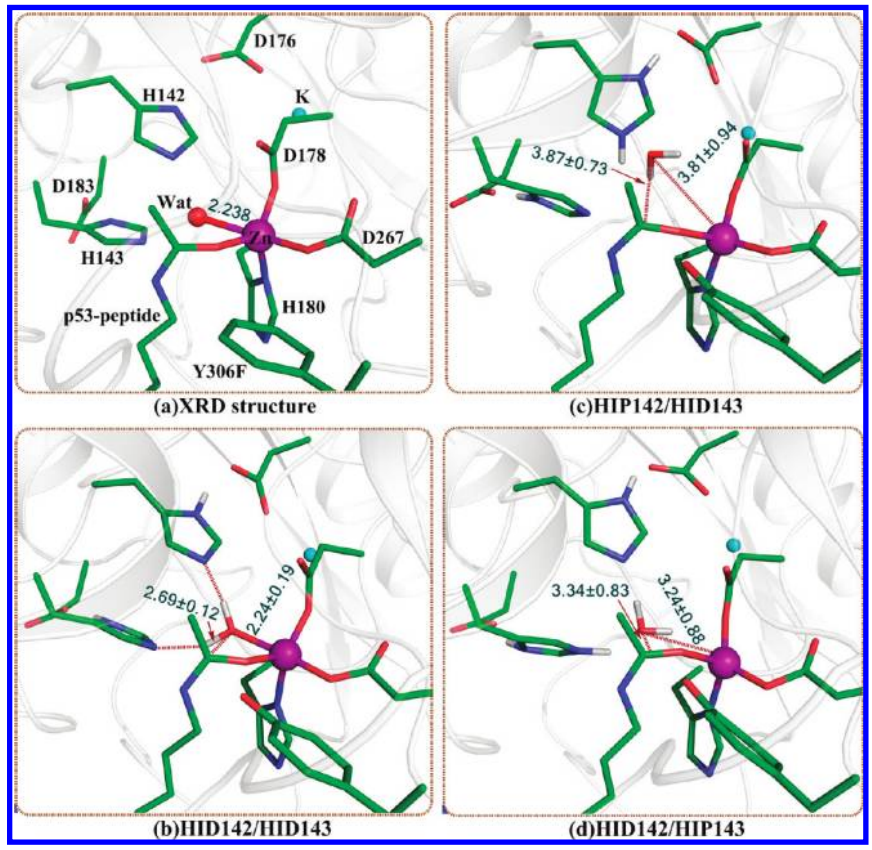

Figure 3. Zinc coordination comparison among the X-ray experimental structure,[24] and various models of the reactant complex after ab initio QM/MM molecular dynamics simulations.

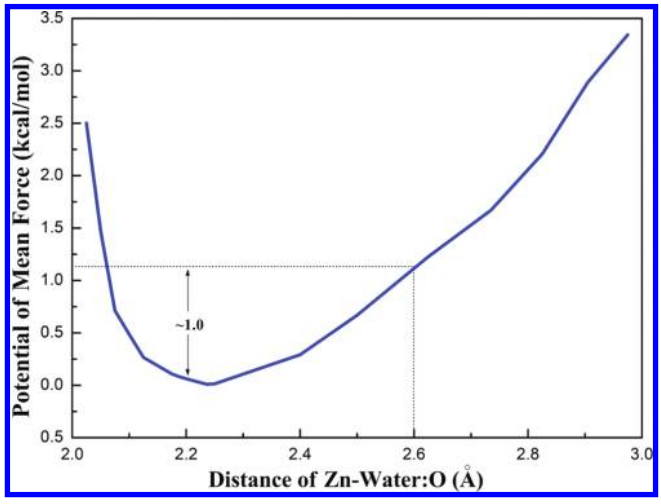

Figure 4. Free energy profile along the zinc−water distance determined ab initio QM/MM MD simulations and umbrella sampling.

the zinc−water oxygen distance. As shown in Figure 4, the free energy profile has a minimum around 2.2 Å, and is quite flat. To elongate the zinc−water oxygen distance to 2.60 Å would only lead to ∼1.0 kcal/mol in free energy change. This further confirms that water is indeed coordinated to Zinc in the HID142/HID143 model, and that this coordination is quite flexible. Thus, our ab initio QM/MM MD simulations have clearly indicated that only the HID142/HID143 model would yield a fivefold Zinc coordination very similar to the one observed in the crystal structure, while in both HIP142/HID143 and HID142/HIP143 models, the water molecule moves away from the zinc ion, leading to a tetrahedral coordination. Furthermore, in the HID142/HID143 model, the distance between the water oxygen and the carbonyl carbon of the substrate is 2.69 ± 0.12 Å, which indicates that this Zinc-activated water molecule is nicely positioned for the nucleophilic attack of the acetyl-lysine. On the other hand, the corresponding distances in other two models are 3.87 ± 0.73 and 3.34 ± 0.83 Å, respectively. All of these suggest that the HID142/HID143 model would be the most reasonable for the reactant complex, but the possibility of the HID142/HIP143 model cannot be completely ruled out as shown in Figure 3. We can see that, although the water molecule is not directly bound to the zinc ion, it is still reasonably well positioned to attack the carbonyl carbon facilitated by His142 as the general base, as suggested in Scheme 1. Accordingly, we have carried out ab initio QM/MM MD simulations and umbrella sampling to determine the free energy profile of its first nucleophilic addition step as illustrated in Scheme 1 for the HID142/HIP143 model. Our calculation shows that the reaction barrier for this step is 29.9 kcal/mol (see Figure S2 in Supporting Information) which is not consistent with the experimental activation barrier of ∼17.7 kcal/mol.[26] This further indicates that the HID142/HIP143 model is not likely to be the HDAC8 reactant complex, and thus, our results do not support the general acid−base catalytic pair mechanism[5] for HDAC8 (Scheme 1 in Figure 2).

3.2. Deacetylation Reaction Mechanism. Our simulations so far have determined the reactant complex of HDAC8, in which both histidine residues in the second Zn^{2+} coordination shell (His142 and His143) are singly protonated. The next essential task is to computationally characterize its deacetylation reaction mechanism. By employing ab initio QM/MM MD simulations and umbrella sampling, we have determined the complete free

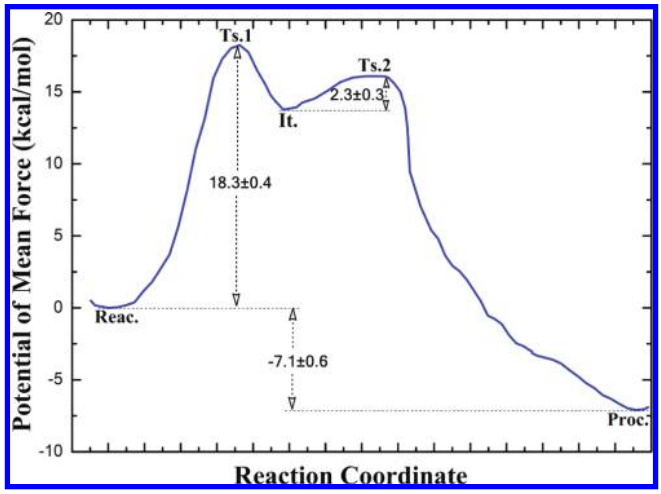

Figure 5. Complete free energy profile for the HDAC8 deacetylation reaction determined by ab initio QM/MM MD simulations and umbrella sampling. The statistical error is estimated by averaging the free energy difference between 5−15 ps and 15−25 ps. The chosen reaction coordinate (RC) for each reaction step was illustrated in Figure S3.

energy profile of the whole deacetylation reaction catalyzed by HDAC8, as shown in Figure 5. We note that the overall reaction includes two reaction steps with a metastable intermediate, and the first step is the rate-determining step. The resultant product state has a lower free energy than the reactant state, indicating that the overall deacetylation reaction is thermodynamically favorable. The calculated overall free energy activation barrier is 18.3 ± 0.4 kcal/mol, which is consistent with the experimental value of 17.7 kcal/mol estimated from the k_{cat} value[26] of 0.90 ± 0.03 s^{-1} for HDAC8 with the transition state theory.

The active-site structures of determined reactant, transition states, and intermediates as well as the characterized reaction mechanism are illustrated in Figure 6, and key geometries are labeled. At the state of reactant, the reactive water molecule, which is coordinated to the zinc ion and hydrogen-bonded to both His142 and His143, is well positioned to nucleophilic attack the carbonyl carbon of the acetyl substrate. In the initial reaction step, the nucleophilic attack of the water to the carbonyl carbon of the acetyl substrate is concerted with the proton transfer from water to His143, and forms a tetrahedral intermediate. Following the proton transfer from His143 to the amide nitrogen breaks the amide bond to produce the lysine and acetic acid products. Meanwhile, as shown in Figure S4, the hydrogen bond between acetic acid and His142 breaks after the second transition state and the proton spontaneously transfers from acetic acid to His143. During the whole reaction process, the essential role of His143 is clearly demonstrated: it acts first as a general base to abstract a proton from the reactive water molecule, and then as a general acid to deliver the proton to the leaving group. While for His142, it does not directly participate in the reaction, but facilitates the reaction by hydrogen bonding with the reactive water molecule during the initial stage of the deacetylation reaction.

From Zn−ligand distances (d_1−d_5) shown in Figure 6, we note that only d_4 (the distance between Zn and the oxygen atom of water) was significantly elongated from 2.24 ± 0.19 Å (the reactant) to 2.71 ± 0.17 Å (the product) during the deacetylation process, while other four interaction distances in the Zn coordination sphere are less changed. The fivefold coordinated Zn in HDAC8 can survive only at the initial reaction step, and it evolves into a tetrahedral configuration at the intermediate state and the rest of the deacetylation process. This initial penta-coordination enables the Zn^{2+} ion to play multiple catalytic roles to facilitate this rate-determining step, including the activation of the zinc-bound water nucleophile, serving as a Lewis acid to polarize the carbonyl group, and stabilizing the oxyanion formed at the transition state.

Figure 6 presents selected key hydrogen bond distances in the active site during the reaction process. We note that the two hydrogen bonds between the conserved His−Asp dyads (His142−Asp176 and His143−Asp183) are very stable and they always exist along the deacetylation pathway. Asp101 and Tyr306 are two strictly conserved among all class I HDACs.[28,74] Both oxygen atoms of Asp101 can form hydrogen bonds with the backbone amides of substrate at the reactant and intermediate states, but only one hydrogen bond interaction survives at the product state. Such weakening of hydrogen bond interactions would facilitate the release of product from the active site. Tyr306 forms a hydrogen bond with the carbonyl oxygen of the acetyl group at the reactant state with an H···O distance of 1.96 ± 0.15 Å. During the reaction process, this hydrogen bond at the transition state and the intermediate is significantly short, compared to the reactant state. This enhancement of hydrogen bond interaction stabilizes the transition state and intermediate. At the product state, this hydrogen bond becomes notably weak with an H···O distance of 2.18 ± 0.41 Å, which would facilitate the leaving of the acetic acid product from the active domain. Such chameleon features of this hydrogen bond lend support for the catalytic role of Tyr306.

3.3. Functional Role of K^+ Near the Active Site. One most intriguing mechanistic question regarding HDAC8 is the function of the K^+ ion near the Zn^{2+} catalytic site, as illustrated in Figure 1. This K^+ ion binding site is conserved among most class I and II HDACs, but does not exist in HDLP. To directly investigate its effect on the deacetylation, we have employed the same computational protocol to prepare and simulate a HDAC8−substrate complex model without the K^+ ion near the active site, which is denoted as the without-K^+ model. By employing the same ab initio QM/MM MD simulations and umbrella sampling, we have determined the free energy profile for the first reaction step, which is the rate-determining step for the wild-type enzyme. As shown in Figure 7, the absence of the K^+ ion results in a free energy barrier of 22.6 ± 0.5 kcal/mol, 4 kcal/mol higher than the wild-type enzyme, showing that the K^+ ion plays an important catalytic role in the deacetylation process by HDAC8. This is consistent with the observed potassium dependence of HDAC8 on the deacetylation activity.[27,75]

To elucidate the functional role of K^+, we compared the active site structures between the wild-type and the model without K^+ as shown in Figure 8. At the reactant state, although the coordination interaction with K^+ would change the orientation of Asp176, the hydrogen bond network in the active site and the fivefold zinc coordination shell are quite similar between two models. The notable difference in the zinc coordination is found to be the zinc−substrate distance, which is longer and more flexible in the model without K^+ (2.23 ± 0.13 Å), compared to that in the wild-type (2.13 ± 0.06 Å). This indicates

(74) Schafer, S.; Saunders, L.; Eliseeva, E.; Velena, A.; Jung, M.; Schwienhorst, A.; Strasser, A.; Dickmanns, A.; Ficner, R.; Schlimme, S.; Sippl, W.; Verdin, E.; Jung, M. *Bioorg. Med. Chem.* **2008**, *16*, 2011–2033.
(75) Hu, E.; Chen, Z. X.; Fredrickson, T.; Zhu, Y.; Kirkpatrick, R.; Zhang, G. F.; Johanson, K.; Sung, C. M.; Liu, R. G.; Winkler, J. *J. Biol. Chem.* **2000**, *275*, 15254–15264.

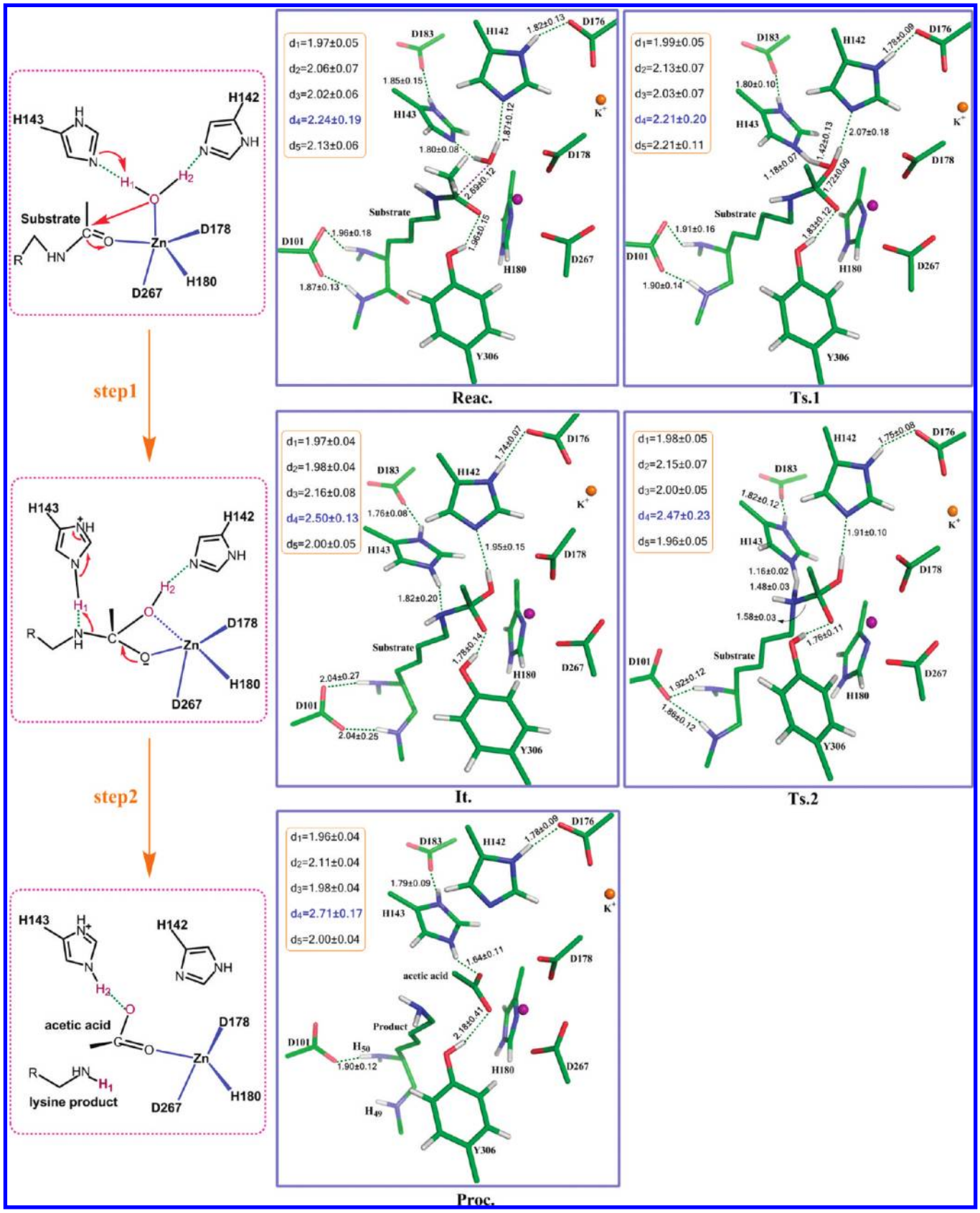

Figure 6. The characterized proton-shuttle deacetylation reaction mechanism and active site geometries at determined reactant, transitions states, intermediate, and product states. (The distances are in Å, and the interaction distances (d_1−d_5) in the Zn coordination sphere refer to Figure 1c.)

that the substrate binding becomes weak without the presence of K^+ near the active site. For the intermediate state, as seen from Figure 8, except that His143 is more suitably placed to mediate the proton transfer to the leaving group in the wild-type model, both models also have similar structures of the active site. Interestingly, at the transition state, two models

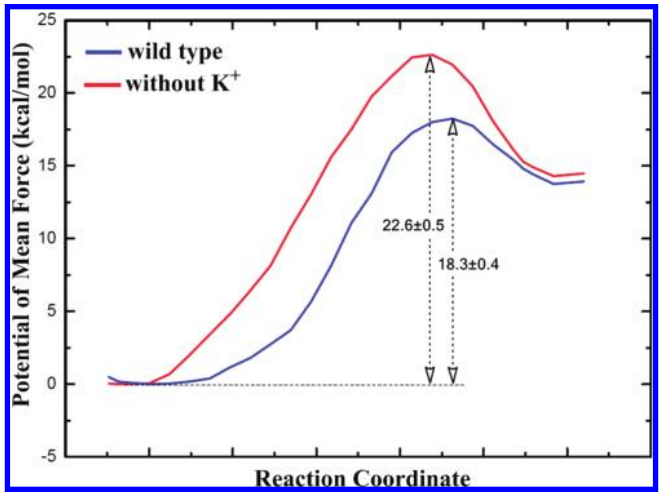

Figure 7. Free energy profiles for the rate-determined step (step 1) of deacetylation reaction in HDAC8 for both the wild-type and the model without the K^+ close to the active site.

exhibit significant differences in the Zn^{2+} coordination and hydrogen bond interaction of the His143−Asp183 dyad. For the wild-type model, Zn^{2+} is fivefold coordinated with d_4 of 2.21 ± 0.20 Å (the distance between Zn and the oxygen atom of water) and the hydrogen bond of the His143−Asp183 dyad is stable with an H···O distance of 1.80 ± 0.10 Å. However, for the model without K^+, Zn^{2+} has a fourfold coordination with d_4 of 2.56 ± 0.18 Å, and the hydrogen bond of the His143−Asp183 dyad is broken with an H···O distance of 3.22 ± 0.21 Å at the transition state. It should be noted that the broken hydrogen bond of the His143−Asp183 dyad at the transition state is reformed at the intermediate state, and the breaking and making of this hydrogen bond were found to proceed consecutively along the reaction pathway, as shown in Figure S5. Meanwhile, we have computed the interaction energies between the QM subsystem and its environment at the reactant, the transition state, and the intermediate for both

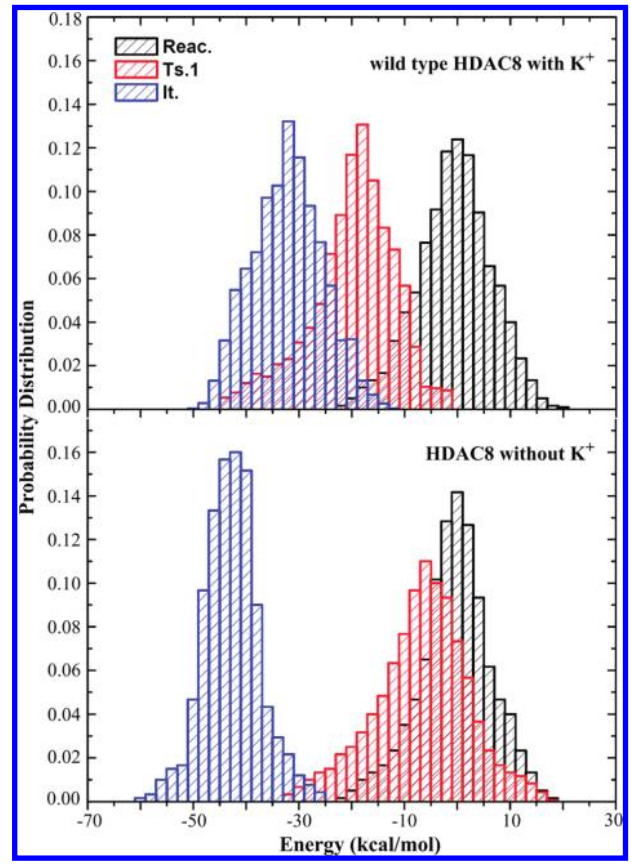

Figure 9. Calculated electrostatics and van der Waals interaction energies between the QM subsystem and its environment at the reactant, the transition state, and the intermediate for first reaction step. Note that the average energy contribution at the reactant for each model has been shifted to zero and the corresponding values are shifted for the transition state and the intermediate.

systems, as shown in Figure 9. We note that the environment can stabilize the transition state more remarkably in the wild-

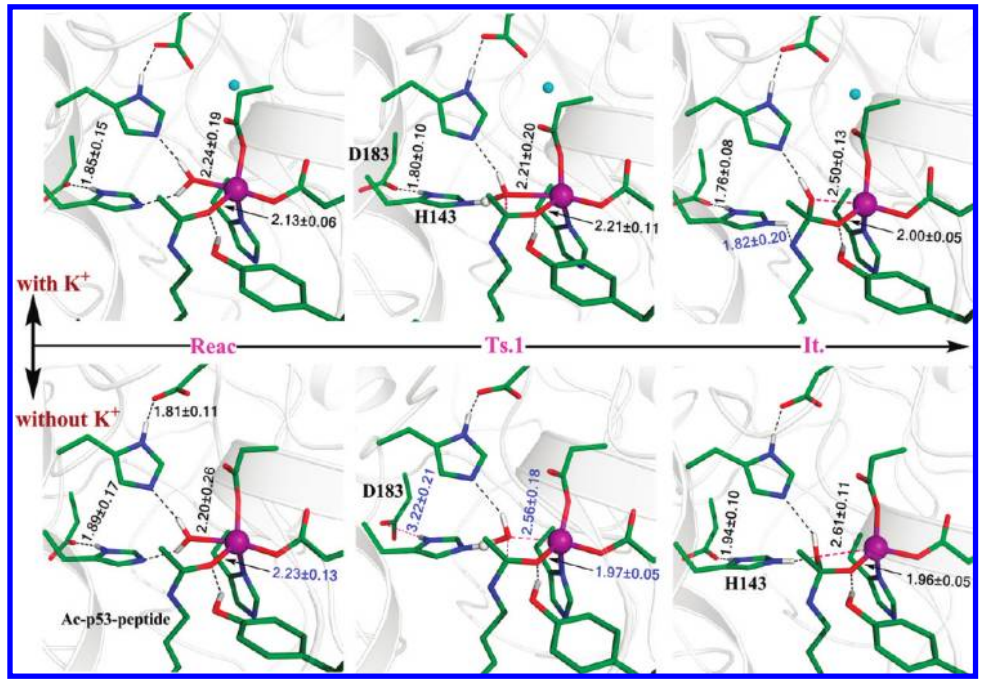

Figure 8. The active site structures of with/without K^+ HDAC8 models along the rate-limited step. The hydrogen bonds are shown by dash line in black.

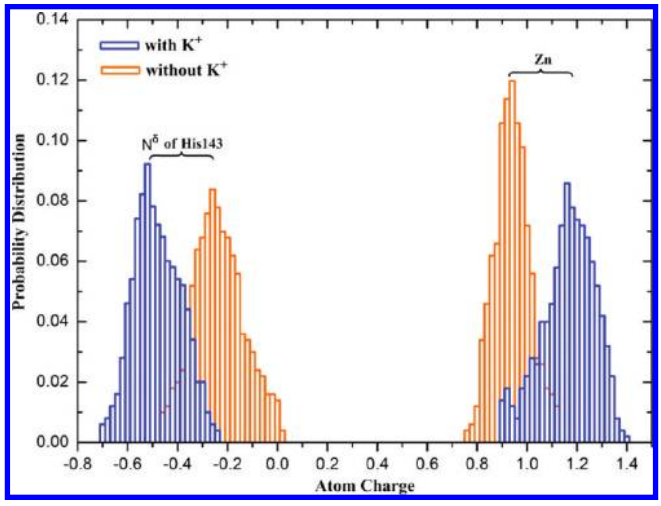

Figure 10. Charges on selected atoms at the reactant state of HDAC8 for the wild-type model and the model without K^+ close to the active site.

type HDAC8 than that in the model without K^+, while its contribution to stabilization of the intermediate is quite similar for both models. These results are consistent with the calculated free energy profiles, in which there are distinct free energy barriers and similar relative free energy changes from the reactant to the intermediate.

To further provide insights into catalytic effect of K^+ in HDAC8, we have analyzed the partial charges on the Zn^{2+} ion and the nitrogen atom (N^{δ}) of His143 at the reactant state to examine how the existence of the K^+ ion affects their catalytic roles. As Figure 10 shows, the presence of K^+ would significantly increase the positive charge on Zn^{2+} and the negative charge on nitrogen atom (N^{δ}) of His143. The more positive charge on the Zn^{2+} would make it more powerful to activate its bound water nucleophile and serve as a stronger Lewis acid to polarize the carbonyl group. Meanwhile, His143 serves as a general base to accept a proton from the Zn-coordinated water molecule, and the more negative charges on nitrogen atom (N^{δ}) would make it become a stronger base. Thus, our results show that the existence of K^+ ion in HDAC8 increases the basicity of His143 and enhances the catalytic role of Zn^{2+}.

4. Conclusions

On the basis of extensive Born−Oppenheimer ab initio QM/MM MD simulations, a proton-shuttle mechanism for HDAC8 was determined, and the functional role of the K^+ ion close to the active site was elucidated. Our simulations indicated that both His142 and His143 are neural and singly protonated at the Michaelis reactant complex. His143 serves as the general base to accept a proton from the zinc-bound water molecule in the initial rate-determining nucleophilic attack step, and then acts as a general acid to deliver the proton to the leaving group to facilitate the cleavage of the amide bond. During the deacetylation process, the Zn^{2+} ion has a dynamic coordination and plays multiple roles to facilitate the reaction. For the K^+ ion near the Zn^{2+} catalytic site, our results revealed its functional importance and suggested that its existence would strengthen several key catalytic elements in HDAC8, including the substrate binding, the His143−Asp183 dyad, the basicity of His143, the catalytic role of zinc ion, and the transition state stabilization by the enzyme environment. It should be noted that our simulation studies here focus on the zinc-dependent HDAC8; thus, some caution should be exercised to extend these results to other HDACs. Meanwhile, our current study demonstrated the viability and powerfulness of Born−Oppenheimer ab initio QM/MM MD simulations in elucidating inner workings of metalloenzymes.

Acknowledgment. This work was supported by NIH (R01-GM079223), NSF (CHE-CAREER-0448156), and the China Scholarship Council. We thank NCSA and NYU-ITS for providing computational resources. We also thank Dr. Po Hu for helpful discussions.

Supporting Information Available: The detailed QM/MM partition scheme; the free energy reaction profile for the first reaction step of the HID142/HIP143 model; illustration of the reaction coordinate (RC) chosen for each step of the reaction in the ab initio QM/MM studies; the change of hydrogen bond between H2 of water and His142/His143 during the deacetylation reaction, and the change of hydrogen bond distance between Asp183 and His143 along the rate-determining step in with/without K^+ models; complete refs 22, 46 and 70. This material is available free of charge via the Internet at http://pubs.acs.org.

JA103932D